A Nature Portfolio journal



https://doi.org/10.1038/s43247-025-02553-1

# Shift in phytoplankton community composition over fronts

Check for updates

Marina Lévy ® ¹ ⋈, Clément Haëck ® ¹, Inès Mangolte², Angelina Cassianides ® ¹ & Roy El Hourany ® ³

Oceanic fronts often support enhanced phytoplankton biomass. Yet, how fronts influence the composition of phytoplankton communities remains poorly understood. Here, we leverage 18 years of high-resolution satellite data of sea-surface temperature and ocean color-derived pigments, converted into concentrations of seven phytoplankton groups, including diatoms, prokaryotes, and five other eukaryotic groups, to examine changes in phytoplankton community composition over fronts across oligotrophic to eutrophic conditions in the Northwest Atlantic. We found a population shift towards more diatoms and less prokaryotes at fronts, while the change in proportion of the other eukaryotic groups varies. This shift accounts for up to a half of the large-scale community dissimilarity, underscoring the substantial influence of fronts on phytoplankton community composition. Our findings suggest that fronts may serve as natural diatom refuges in a warming climate, highlighting the necessity of incorporating fine-scale oceanographic features like fronts into climate models.

Phytoplankton are an extremely diverse group of microscopic marine organisms unified by their ability to photosynthesize<sup>1</sup>. They form the basis of the marine food web and drive biogeochemical cycles, including those of carbon, nitrogen and oxygen<sup>2</sup>. The structure and composition of phytoplankton communities are critical for determining the efficiency of these cycles<sup>3–7</sup>, for ecosystem functioning<sup>8–10</sup>, and for shaping marine food web dynamics<sup>11</sup>; they are indicators of the global ocean's state and health<sup>12,13</sup>. Different metabolic strategies enable various phytoplankton groups to adapt to their unique environmental niches: diatoms, for example, thrive in nutrient-rich but variable environments<sup>14,15</sup>, while prokaryotes have efficient nutrient uptake at low concentrations<sup>16,17</sup>. Thus on a regional scale, sharp contrasts exist between the eutrophic, subpolar regions characterized by intense nutrient delivery by winter convection which are favorable for diatoms<sup>14,15,18</sup>, and the highly stratified, nutrient poor subtropical regions which are generally dominated by prokaryotes such as cyanobacteria<sup>19–22</sup>.

Fronts are ubiquitous fine-scale features in the ocean marked by sharp horizontal gradients in water properties (such as temperature, salinity and nutrients)<sup>23</sup>, which can be either quasi-persistent and locked in place by the coastal boundary and large-scale atmospheric forcing, or ephemeral and continuously forming, moving, and dissipating at the ocean surface through interaction between mesoscale eddies<sup>24</sup>. Importantly, a front will generate a cross-frontal overturning circulation and an along-front circulation<sup>25,26</sup>. These frontal circulations facilitate vertical and horizontal nutrient transport<sup>24,27,28</sup>, creating favorable conditions for larger phytoplankton, such as diatoms, to flourish over the front. While previous studies have primarily reported localized increases in diatoms at specific fronts and times<sup>14,29–36</sup>, the

broader, cumulative impact of fronts on the entire phytoplankton community structure at the regional scale of biogeochemical provinces and the temporal scales of seasons remains under-explored<sup>37</sup>.

Recent advancements in the analysis of satellite ocean color data have improved our ability to quantify phytoplankton biomass at fine spatial and temporal scales over broad provinces<sup>38–40</sup>, and has demonstrated that phytoplankton biomass was increased over fronts at the regional and seasonal scales in the open ocean<sup>41,42</sup>, a result confirmed with bio-argo in-situ data<sup>43</sup>. But these previous work have focused primarily on total biomass changes; there remains a critical need to understand how these changes in total biomass translate into shifts in community composition. Building on these capabilities, we use an existing two-step approach<sup>44</sup>, in which satellite ocean color data are first used to estimate the concentrations of seven pigments via a self-organizing map (SOM), which are then converted into the relative Chl-a concentration of seven phytoplankton groups—including diatoms, five other eukaryotic groups, and a broad group of prokaryotes—using diagnostic pigment analysis<sup>45</sup>.

By combining these satellite-derived pigments and group concentration estimates, with fronts and their associated phytoplankton anomalies located daily from an index based on sea-surface temperature (SST) heterogeneity<sup>42</sup>, we provide new insights into the influence of oceanic fronts on phytoplankton community structure across the North Atlantic.

This study area spans three major North Atlantic biomes—subpolar, seasonal subtropical, and permanent subtropical—characterized by a gradient from oligotrophic to eutrophic conditions (Fig. 1A), and with a sharp increase in the proportion of diatoms along this gradient (Fig. 1F and

<sup>1</sup>Sorbonne Université, LOCEAN-IPSL, CNRS, IRD, MNHN, Paris, France. <sup>2</sup>ENTROPIE, IRD, CNRS, UR, UNC, Ifremer, Noumea, New Caledonia. <sup>3</sup>LOG, Univ. Littoral Côte d'Opale, Univ. Lille, CNRS, IRD, Wimereux, France. e-mail: marina.levy@locean.ipsl.fr

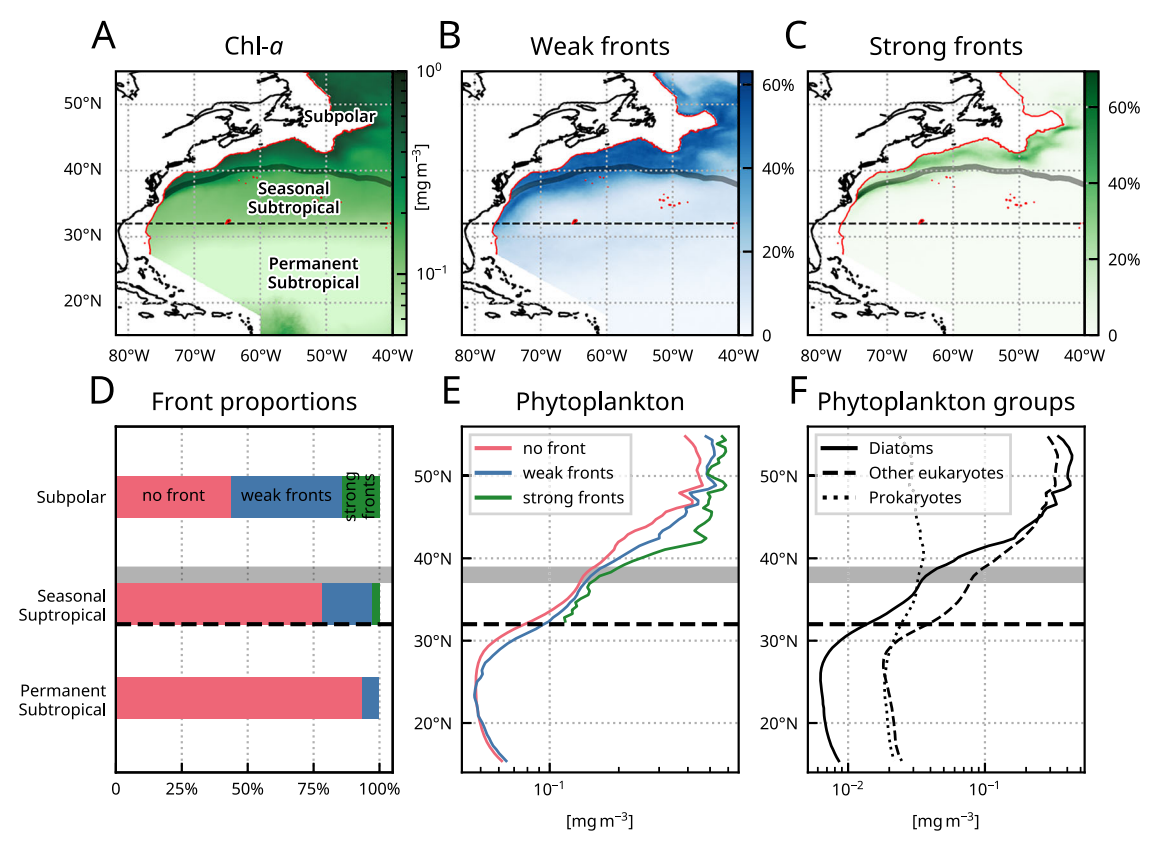


**Fig. 1** | **Large-scale context of study region.** Climatological distribution over 2002–2020 of (**A**) Phytoplankton (in mg Chl-a  $m^{-3}$ ), **B**, **C** occurrence of weak (resp. strong) fronts (expressed in percent of time a pixel is occupied by a weak/strong front), **D** relative occurrence of background (non front), weak front and strong front in each biome, **E** meridional transect (averaged over 40–45°W) of phytoplankton concentration (in mg Chl-a  $m^{-3}$ ) in the background (no front) and over weak and strong fronts, **F** same transect for the relative proportion of phytoplankton sorted

into three groups. Latitudinal profiles similar to those shown in panels (E) and (F), covering each of the seven phytoplankton groups and their associated diagnostic pigments, are presented in Supplementary Fig. 1. In (A), the red line marks the continental shelf and values over the shelf have been masked. The thick gray line and dashed line represent the climatological boundaries between the permanent subtropical, seasonal subtropical and subpolar biomes.

Supplementary Fig. 1). It is characterized by strong quasi-permanent fronts associated with the Gulf Stream and numerous weaker and more ephemeral fronts driven by the intense mesoscale activity resulting from the instability of the Gulf Stream (Fig. 1B–C), which are associated with an increase in total phytoplankton biomass [and Fig. 1E<sup>42</sup>]. The present analysis shows that this biomass enhancement is not evenly distributed across the phytoplankton community, and that diatoms generally benefit more than the other groups, although other eukaryotic phytoplankton can also experience substantial, and in some cases greater, increases depending on the conditions.

We further examine whether this change in phytoplankton community composition at fronts mirror larger regional-scale transitions across the three biomes. Specifically, we quantify shifts in community structure over weak and strong fronts throughout the year and compare these changes to regional differences observed among the biomes. Such insights are essential for understanding the role of fronts in modulating marine biodiversity and their broader implications for ecosystem functioning and carbon cycling at regional scale.

#### Results and discussion

#### Changes in phytoplankton communities over individual fronts

Individual satellite images in our dataset illustrate the notable influence of oceanic fronts on phytoplankton distribution. For example, Fig. 2 highlights a complex interplay of intertwined and merging sea surface temperature (SST) fronts in the subpolar biome, as indicated by heterogeneity index values exceeding 5 (refer to Materials and Methods). As part of it, the area marked "Front 1", situated in the lower right corner of the image, corresponds with a marked Chl-a peak, predominantly driven by diatoms,

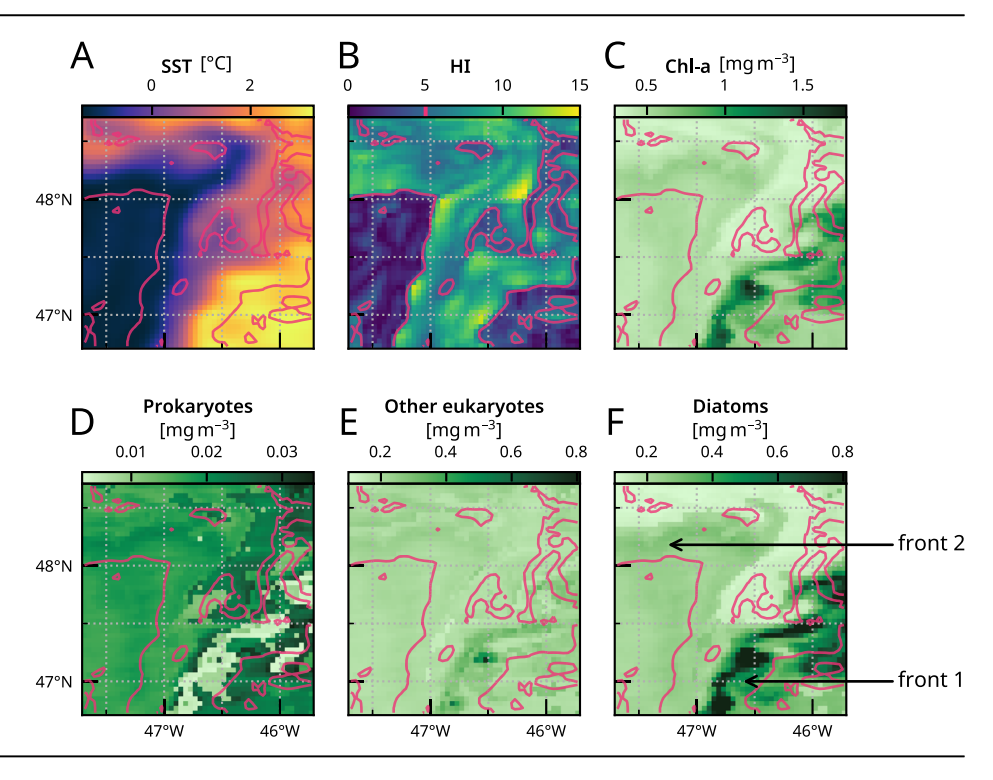
alongside a smaller contribution from other eukaryotes and a low presence of prokaryotes. In the continuity of Front 1, the area marked "Front 2" extends horizontally above 48"N and forms an elbow-like curve. It exhibits a weaker, yet discernible Chl-a maximum distributed among all three phytoplankton groups. Similar examples in the seasonal subtropical and permanent subtropical biomes are shown in Supplementary Figs. 2–3.

## Statistical changes in phytoplankton communities over multiple fronts

While individual images provide insight into the spatial configuration of these fronts and their local impact on phytoplankton community composition, it is through the analysis of 18 years of data that we are able to quantify their impact on a regional scale, across three biomes and throughout the year. This long-term dataset reveals more consistent patterns and offers a more robust quantitative assessment than is possible with single images or in-situ surveys, which are inherently restricted to a limited number of observations <sup>36,46–49</sup>.

The dataset reveals clear regional contrasts. In the subpolar biome, phytoplankton dynamics are characterized by a prominent spring bloom dominated by diatoms. In contrast, the perennial subtropical biome is characterized by consistently higher levels of prokaryotes and other eukaryotes (Fig. 3 and Supplementary Fig. 1). This marked biogeographical contrast has been previously documented through various approaches: satellite-based assessments of dominant phytoplankton types at the global scale<sup>50,51</sup>; meridional transects of pigment composition and size structure in the Atlantic Ocean<sup>52,53</sup>; global analyses of phytoplankton phenology using ocean color data<sup>54</sup>; metabarcoding and metagenomic analysis over the global

Fig. 2 | Examples of front's influence on phytoplankton communities. Satellite snapshot of (A) SST and (B) its associated Heterogeneity Index (HI), of (C) total Chl-a concentration and of the relative concentrations of (D) prokaryotes, (F) diatoms and of (E) the sum of five other eukaryotes in the subpolar biome. Note a different color scale is used for prokaryotes. Frontal regions are delineated by the red contour, which corresponds to a HI threshold of 5. The labels "Front 1" and "Front 2" highlight two distinct frontal features: one oriented north-south (Front 1) and the other oriented east—west (Front 2). Both features are visible in the sea surface temperature (SST) field and converge in the upper right corner of the panel.



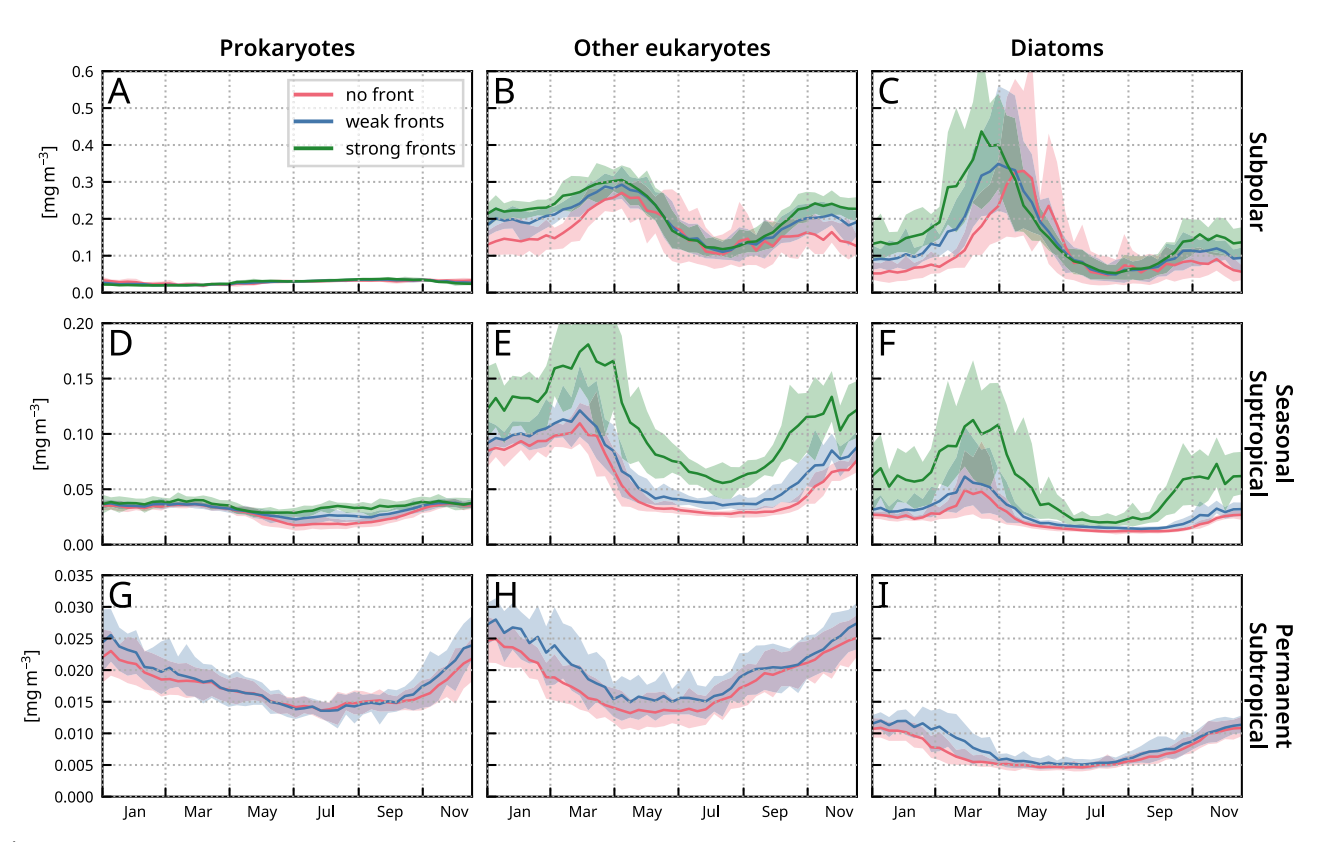


**Fig. 3** | **Seasonal influence of fronts on phytoplankton communities.** Climatological seasonal cycles of (**A**, **D**, **G**) Prokaryotes, (**C**, **F**, **I**) Diatoms and (**B**, **E**, **H**) the other eukaryotes in the (**A**–**C**) subpolar, (**D**–**F**) seasonal subtropical and (**G**–**I**) permanent subtropical biomes, in the background (no front, red), over weak fronts

(blue) and over strong fronts (green). The plain lines represent the climatological mean over the period 2002-2020 of the median of 8-day distributions. The envelopes mark the 10% and 90% percentile of the climatological spread over the period 2002-2020.

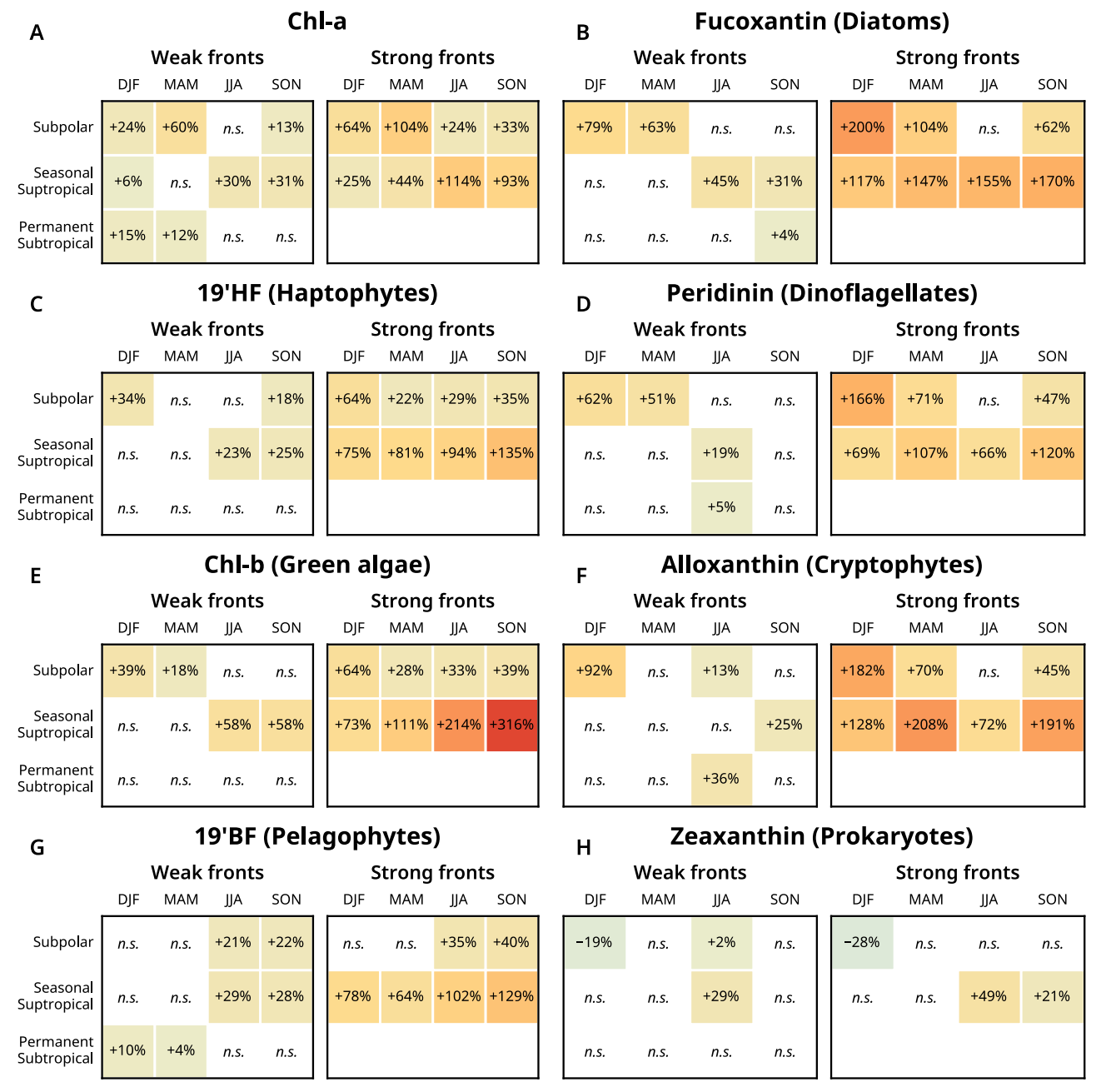


**Fig. 4** | Quantification of the impact of fronts on phytoplankton pigments. Relative increase of the mean concentration of total Chl-a (**A**) and of the seven diagnostic pigments (**B**–**H**) in weak and strong fronts compared to the background, by season and for each biome. The shade of cells is proportional to the increase. Cells

where the concentration distributions in and outside fronts are not significantly different (p-value threshold of 0.05) are marked "n.s". Errors in these estimates due to the propagation of pigment estimated uncertainties<sup>44</sup> are less than 0.01%.

ocean<sup>55,56</sup>; and global models of phytoplankton diversity<sup>57</sup>. Positioned between these two contrasting regimes, the seasonal subtropical biome displays intermediate phytoplankton biomass levels and an earlier spring bloom onset. This is consistent with phenological patterns observed in the North-East Atlantic from ocean color data<sup>58</sup>, and with the presence of other eukaryotic taxa reported from optical imaging studies and metabarcoding along similar latitudinal gradients in the North and South Pacific<sup>59-61</sup>.

This contrast between the three biomes is thought to be related to variations in nutrient supply. Wind-driven patterns of Eulerian mean vertical velocities are characterized by upwelling in the subpolar gyre and downwelling in the subtropical gyre<sup>62</sup>, leading to a shallower nutricline and a more productive regime in the north, triggered seasonally by the winter deepening of the mixed layer; but in the subtropical gyre, south of the Gulf

Stream extension, the deeper nutricline and weak winter convection lead to perennial oligotrophy<sup>63</sup>, although in the seasonal subtropical region just south of the Gulf Stream flank, lateral nutrient inputs<sup>64</sup> and deeper convective mixing<sup>65</sup> allow more productivity.

Our findings demonstrate a consistent enhancement in surface Chl-a concentration over fronts compared to non-front conditions across the three biomes and throughout the year (Fig. 3), although the magnitude of this enhancement varies between phytoplankton groups. This increase is more pronounced over strong fronts than weak ones, with particularly notable responses from diatoms and other eukaryotes, while prokaryotes exhibit a minimal and often barely detectable increase. A careful calculation of the statistical significance of the percent increase in associated pigments confirms this general trend (Fig. 4). Marked increases are more frequent

over strong fronts compared to weak ones. When examining pigments individually, we find that, in addition to Fucoxanthin (diatoms), Chlorophyll-*b* (green algae) and Alloxanthin (cryptophytes) show the most pronounced enhancement over fronts, with 19'HF (haptophytes), Peridinin (dinoflagellates) and 19'BF (pelagophytes) also increasing, albeit to a lesser extent. Moreover, surface enhancements are often negligible during the summer months (JJA) and within the permanent subtropical gyre, when the water column is more stratified and biomass often located below the surface. We can also note a statistically significant decrease of the prokaryotes at fronts, detectable in winter in the subpolar region.

The observed enhancement of diatoms in both eutrophic and oligotrophic biomes aligns with previous in-situ observations from various regions of the global ocean<sup>30,31,36</sup>, as well as artificial nutrient-loading experiments<sup>66</sup>, model results<sup>67-69</sup> and satellite studies<sup>35</sup>. Although we cannot directly link specific physical processes to their biological impacts, existing literature suggests that diatom enhancement is likely driven by increased aperiodic nutrient supplies<sup>66</sup>, facilitated through either vertical<sup>24</sup> or horizontal transport<sup>70</sup>.

The impact of fronts on the other eukaryotes is less extensively documented, except in cases such as dinoflagellate red tides forming at fronts<sup>71,72</sup> and the association of coccolithophores<sup>73,74</sup> and haptophytes (phaeocystis bloom<sup>61</sup>) with major fronts in the Southern Ocean. Remarkably, an overall increase in eukaryotic richness across large-scale fronts in the South Pacific was previsouly reported<sup>59</sup>.

The effects of fronts on prokaryotes are even less clear, likely reflecting their diverse trophic strategies and varied responses based on specific traits. For example, some studies have reported *Prochlorococcus* and *Synechococcus* as segregated across fronts<sup>32,47,75</sup>, or distributed differently within and outside eddies<sup>76</sup>. Other studies have shown increased concentrations of diazotrophs at fronts<sup>48,77</sup> or eddy edges<sup>78</sup>, or decreased cyanobacteria

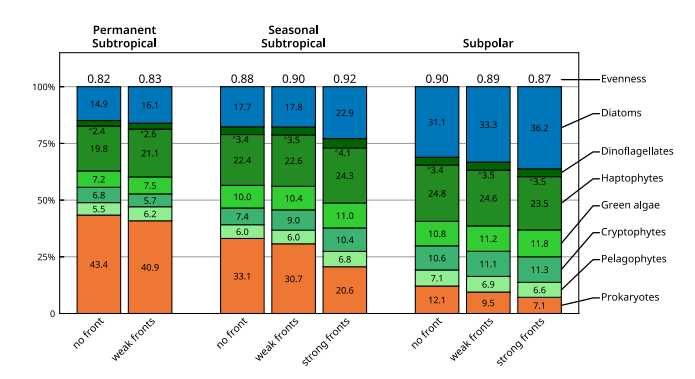


Fig. 5 | Phytoplankton community composition changes associated with fronts across regions. Phytoplankton community composition (relative proportion of Chl-a concentration of the seven phytoplankton groups) with each biome over nonfront, weak fronts and strong front conditions. The percentages (indicated over the colored bars) are computed from the median concentrations over the full range of data (2002–2020). Corresponding evenness values are indicated on top of each bar. Diatoms are in blue, the other eukaryotes in shades of green, and prokaryotes are in orange.

concentrations over fronts<sup>36</sup>. In this latter case, which most closely resembles that observed here, the decrease was likely driven by biotic interactions, as suggested by model simulations<sup>69</sup>.

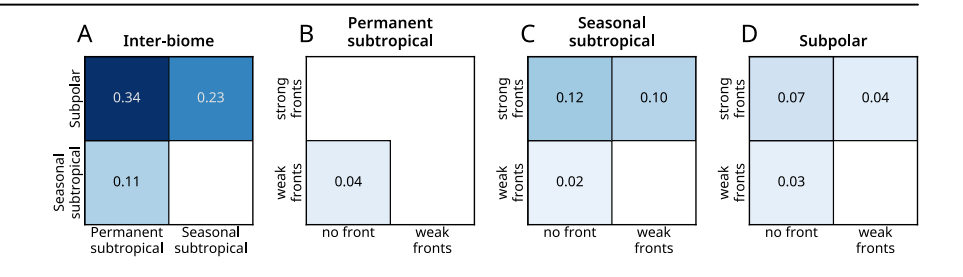
### Statistical shifts in phytoplankton community composition over fronts

It is important to highlight that, unlike many previous studies focusing on individual phytoplankton groups, our approach allowed for a comprehensive assessment of the impact of fronts on the entire phytoplankton community using a consistent methodology. Our findings indicate that while fronts in this region are consistently associated with elevated Chl-a concentrations, the additional biomass is unevenly distributed among the phytoplankton groups. Specifically, fronts result in an increased proportion of diatoms and a reduced proportion of prokaryotes (Fig. 5). This pattern is consistently observed across all three biomes and becomes more pronounced with the increasing strength of the fronts. Regarding other eukaryotes, they increase in proportion in the seasonal subtropical biome, although less markedly than diatoms; in the subpolar biome, green algae and cryptophytes increase slightly in proportion, and the other eukaryotes slightly decrease.

These community shifts in phytoplankton community composition over fronts are similar in sign and magnitude whether the community is examined in terms of phytoplankton groups (Fig. 5) or in terms of pigments (Supplementary Fig. 4). This demonstrates the robustness of the result and suggests that it is not sensitive to the methodology used to derive phytoplankton groups from pigment data. They suggest that eukaryotes are more responsive to the environmental changes associated with fronts compared to prokaryotes. Although the changes in the relative proportions of phytoplankton groups are relatively small—typically less than 5% of the total community composition—they are systematic. This leads to alterations in community evenness (Fig. 5): a decrease in evenness over fronts in the subpolar biome, primarily due to a lower proportion of prokaryotes, and an increase in evenness over fronts in both subtropical biomes, driven by a rebalancing between prokaryotes, other eukaryotes and diatoms.

The shifts in community composition between biomes, and due to fronts within each biome, are illustrated by the step-like patterns in Fig. 5, with progressively smaller steps for prokaryotes (in orange) and larger steps for diatoms (in blue) as we move from left to right. The magnitude of this shift was quantified by comparing the dissimilarity in phytoplankton communities between biomes (Fig. 6A) with the dissimilarity induced by fronts in each biome (Fig. 6B-D). At the regional scale, the two subtropical biomes exhibit smaller dissimilarity to each other (0.11) than to the subpolar biome (0.23 and 0.34). Note that the dissimilarity index ranges from 0 to 1, with higher values indicating greater differences between communities. Within each biome, dissimilarities due to fronts range from 0.02 to 0.12. Although these are generally less pronounced than regional-scale dissimilarities, they are of a similar order of magnitude. An exception is the dissimilarity between no-front and strong front in the seasonal subtropical biome (0.12), which slightly exceeds the dissimilarity between the seasonal subtropical and permanent subtropical biomes (0.11). On average, dissimilarities due to fronts within biomes are about one-quarter of those

Fig. 6 | Comparison of large-scale and frontal-scale phytoplankton community dissimilarities. Dissimilarities in phytoplankton communities, (A) between pairs of biomes (large-scale), and (B–D) within each biome, between pairs of frontal conditions (frontal scale: no front, weak front, strong front). The shades of blue provide a visualization of the magnitude of the dissimilarities (also indicated with numbers between 0 and 1); darker shades of blue (and larger numbers) indicate larger dissimilarity between pairs of phytoplankton communities.



observed between biomes. However, in the case of strong fronts, intra-biome dissimilarities increase to approximately half the magnitude of inter-biome differences.

This comparison demonstrates that front-induced dissimilarities can reach roughly one-quarter to half of the total dissimilarity observed across the Northwest Atlantic basin—a considerable impact given the differences in spatial scales (ranging from 10 to 1000 km). This underscores the substantial role of fronts in reshaping phytoplankton community composition at the regional scale.

#### **Conclusions**

Phytoplankton play a central role in climate and marine foodwebs, and the impact of climate change will depend heavily on their responses<sup>79</sup>. Our results support the hypothesis that oceanic fronts may serve as refuges for certain phytoplankton groups<sup>15</sup>, such as diatoms. This role could become critically important in the context of climate change, potentially counterbalancing the predicted shift toward others, and often smaller, phytoplankton groups<sup>80–84</sup> and mitigating the resulting trophic amplification effects<sup>85,86</sup>. Consequently, fronts may play a vital role in the future functioning of marine ecosystems by sustaining ecosystem services provided by diatoms<sup>87</sup>, and areas naturally covered with fronts represent promising targets for the establishment of marine protected areas<sup>88–90</sup> and for sustainable fisheries<sup>91</sup>.

However, the extent to which fronts can fulfill this potential will depend on the impacts of climate change on fine-scale ocean dynamics, which remain highly uncertain 38,92-96. Moreover, the role of phytoplankton in trophic transfer and carbon export does not only depend on the trophic group, but also on cell size; diatoms can vary considerably in cell size and play different roles in carbon export and trophic transfer depending on size 98,99. In addition, we have found that not only diatoms, but also other micro and nano eukaryotic groups were favored at fronts. To fully evaluate the global-scale influence of fronts on phytoplankton in the future under various climate change scenarios, it will be essential to incorporate higher taxonomic, size and spatial resolution into Earth System Models than what is currently available.

#### Methods and data Biomes

Our region of interest is the Northwest Atlantic between 15°N and 55°N and west of 40°W, which we divide into three biomes. This vast region extends from the cold, nutrient-rich subpolar gyre to the warm, oligotrophic waters of the subtropical gyre. It is traversed by the Gulf Stream, which marks a clear moving boundary between the subtropical and subpolar gyres. The region is characterized by a north-south gradient in Chl-a throughout the year, resulting from the highly contrasting and well-known production regimes of the North Atlantic<sup>100</sup>: a subpolar biome in the subpolar gyre, characterized by a spring bloom and strong seasonality of phytoplankton; an oligotrophic, permanent subtropical biome in the southern part of the subtropical gyre, characterized by year-round low Chl-a concentrations; and an intermediate, seasonal subtropical biome over the northern flank of the subtropical gyre.

According to Haëck et al. <sup>42</sup>, the geographic boundary between the two biomes within the subtropical gyre, i.e., the permanent subtropical biome and the seasonal subtropical biome, is set at 32°N; the meanders of the Gulf Stream jet form the moving boundary between the seasonal subtropical biome and the subpolar biome. This second boundary is determined at each time step by thresholding the daily SST map to find the steep SST gradient of the so-called Gulf Stream North-wall <sup>42</sup>. The continental shelf, defined by bathymetry less than 1500 m, was excluded from the analysis to specifically target open-ocean processes

#### Satellite data

SST data were derived from the daily 4 km resolution product version 2.0 distributed by the European Space Agency Sea Surface Temperature Climate Change Initiative<sup>101,102</sup>. We used the spatially interpolated Level 4

product to facilitate the calculation of the Heterogeneity Index (HI, see below), but we only used cloud-free pixels for our analysis and therefore reapplied the cloud mask to the HI after calculation. This dataset allows for the daily detection of front positions, capturing fine-scale fronts while they temporally evolve.

Phytoplankton concentration data were derived from the daily 4 km resolution chlorophyll-a (Chl-a) Level 3 product, distributed by ACRI-ST as part of the Copernicus-GlobColour project<sup>103</sup>. This dataset allows for high-resolution mapping of phytoplankton biomass at the scale of fronts, and supports analysis of spatial-temporal variations across biomes. The use of daily data improves the granularity of our analysis, capturing fine-scale variations linked to frontal dynamics. Although it is available since 1998, we have limited the analysis to the period 2002–2020 to avoid the period covered by a single ocean color sensor, during which the data coverage is much lower. Surface Chl-a data derived from ocean color satellites are an imperfect proxy for phytoplankton biomass, which moreover overlooks subsurface phytoplankton that may also be influenced by fronts<sup>104</sup>, but have the advantage to be synoptic and available at the same spatio-temporal resolution as SST.

#### Satellite retrieval of phytoplankton taxonomic groups

We estimated the concentrations (in mg Chl-a  $m^{-3}$ ) of six distinct eukaryotic phytoplankton groups—diatoms, dinoflagellates, haptophytes, green algae, cryptophytes, and pelagophytes—as well as a single broad group for prokaryotes, using daily satellite-derived pigment data at a spatial resolution of 4 km. These pigment data, spanning the period from 2002 to 2020, were an extension of an existing dataset<sup>44</sup>.

The pigment concentrations were inferred from satellite remote sensing reflectances across multiple wavelengths, sea surface temperature (SST), and chlorophyll-a (Chl-a) concentrations, using a neural network classifier. The neural network was cross-validated against an extensive global dataset of in situ phytoplankton pigment measurements acquired via high-performance liquid chromatography (HPLC). While some pigments were predicted with slightly higher accuracy than others<sup>44</sup> (Fucoxanthin:  $R^2 = 0.87$ ; Chlorophyll-b:  $R^2 = 0.85$ ; Zeaxanthin:  $R^2 = 0.80$ ; Peridinin:  $R^2 = 0.80$ ; 19'-Butanoyloxyfucoxanthin (19BF):  $R^2 = 0.79$ ; Alloxanthin:  $R^2 = 0.76$ ; 19'-Hexanoyloxyfucoxanthin (19HF):  $R^2 = 0.75$ ), overall agreement exceeded 75% (i.e.,  $R^2 = 0.75$ ) across all pigments, with estimation errors remaining below 0.02 mg m<sup>-3</sup> for all.

We estimated the concentrations of the phytoplankton taxonomic groups based on the concentration of group-specific pigments, following an existing diagnostic pigment analysis (DPA) method 45. This approach assumes that the concentration of each group is proportional to the concentration of an associated marker pigment, using the relation Group =  $a \times \text{Pigment}$ . The following pigment-group associations and conversion coefficients (a) were applied: Fucoxanthin for diatoms (a = 1.44), Chlorophyll-b for green algae (a = 1.08), Zeaxanthin for prokaryotes (a = 1.55), Peridinin for dinoflagellates (a = 1.40), 19BF for pelagophytes (a = 0.89), Alloxanthin for cryptophytes (a = 1.94), 19HF for haptophytes (a = 1.04). The a coefficients were drawn from established literature 105-108. To obtain the group's contribution to Chl-a, at each pixel in space and time, the concentration of each phytoplankton group (Group, in  $mg \, m^{-3}$ ) was divided by the total pigment concentration (i.e., the sum of all Group) and multiplied by the total Chl-a concentration.

It is important to acknowledge that pigment signatures do not correspond uniquely to specific taxonomic groups. Many pigments are shared among multiple lineages, and pigment concentrations can vary substantially depending on environmental conditions, physiological state, and photoacclimation strategies of the organisms<sup>109</sup>. As a result, the attribution of pigments to specific taxonomic groups entails a degree of uncertainty. To account for this limitation, we also present some of our results directly in terms of pigment concentrations. Nonetheless, group-level interpretations remain useful for broader ecological insights, as they offer a more intuitive framework for understanding community structure and biogeography, and are used preferentially.

We performed the analysis separately for each of the seven phytoplankton groups. However, to provide a more concise and readable overview, we also grouped the five non-diatom eukaryotes (dinoflagellates, haptophytes, green algae, cryptophytes, and pelagophytes) into a single category. Detailed results for each of these groups are available in Fig. 4 and Supplementary Figs. 1 and 6. While our discussion primarily focuses on the three broad categories—diatoms, other eukaryotes, and prokaryotes—we also comment on the individual results for the five non-diatom eukaryotic groups.

As mentioned before, there are uncertainties associated with the retrieval of phytoplankton groups using the algorithm in ref. 44. These stem from errors in pigment estimation within the algorithm and from the challenges of linking specific pigments to particular phytoplankton groups<sup>105</sup>. Additionally, the algorithm is limited to identifying a single, generic prokaryote group. Nevertheless, it enabled us to perform a quantitative comparison of the changes in phytoplankton community structure at the scale of fronts and at the scale of biomes, with a consistent methodology.

#### Front detection

To detect fronts, we used an updated version<sup>42</sup> of the Heterogeneity Index (HI)<sup>40</sup>. The HI provides a local measure of SST heterogeneity at fine spatial scales. The HI was evaluated at each pixel and time step, over a window with sides of 28 km (7 × 7 pixels at 4 km resolution) centered on the pixel of interest. This window size corresponds to about one-third of the Rossby radius of deformation in this region, and is intentionally larger than the width of fine-scale density fronts associated with stirring and ageostrophic secondary circulation. Accounting for a slightly larger scale is a way to account for the temporal decoupling between fine-scale currents and the response of the planktonic ecosystem. This decoupling may result in phytoplankton patches that are not well localized over temperature fronts and can be displaced by a few kilometers<sup>35,36</sup>. In practice, the HI is computed as the weighted sum of the skewness  $\gamma$ , standard deviation  $\sigma$ , and bimodality B of the SST within the window (HI =  $a(by + c\sigma + dB)$ , where b, c, d are constant normalization coefficients equal to the inverse of the standard deviation of each component, and a is the normalization coefficient such that 95% of the values are below an arbitrary value of 9.5.

We sorted the pixels into those associated with large heterogeneity (HI > 10), with medium heterogeneity (5 < HI < 10), and with small heterogeneity (HI < 5). We repeated this at each time step. We referred to these three HI ranges as the background (i.e., non front), weak fronts and strong fronts, respectively, with the underlying hypothesis that stronger HI represented more intense fronts<sup>42</sup>. The instability of the Gulf Stream is the main source of mesoscale and submesoscale activity in the region, and thus of fine-scale physical heterogeneity. This explains the contrast between the permanent subtropical biome, located away from the Gulf Stream and where 90% of HI values are small and where the large levels of heterogeneity are absent, with the subpolar gyre where large and medium HI ranges are more frequent (Fig. 1D).

Using SST heterogeneity as a proxy for fronts has limitations. Its advantage lies in its simplicity, as it requires only widely available SST data with a spatio-temporal resolution that matches ocean color data. However, it assumes that physical and biological heterogeneities coincide in space and time, overlooking the biological response's time lag<sup>24,55,69,110</sup>. We addressed this issue partly by using a sufficiently wide window to calculate the heterogeneity index, yet this approach likely underestimates the total, time-integrated impact of fronts.

#### Quantification of phytoplankton over fronts

To quantify the influence of fronts on phytoplankton assemblages, we pooled pixels by biome, and within each biome, categorized them based on front types (no front, weak fronts and strong fronts). This process yielded eight distinct pixel pools: two in the permanent subtropical biome (no front, weak fronts), three in the seasonal subtropical biome and three in the subpolar biomes (no front, weak fronts and strong fronts). Each pool gathered a variety of situations (i.e., time, location, HI strength) and was thus

associated with a range of concentrations for each phytoplankton group. Distributions of phytoplankton concentrations within each pool were calculated using 18 years of satellite data. Although the distribution shapes were not strictly unimodal, mean and median values were closely aligned (Supplementary Fig. 5), and we selected median values to represent each distribution. Within each pool, we then assessed the relative proportions of the median values for each phytoplankton group.

To determine whether the medians of the distributions from background, weak fronts, and strong fronts were significantly different, we randomly sampled 200 values from each distribution, treating it as a probability density function. We then applied the two-sided Brunner–Munzel test<sup>111</sup> to compare pairs of samples from the background or fronts (either weak or strong). This test evaluates the null hypothesis that the probability of a random sample from the first distribution X having a higher value than a sample from the second distribution Y is the same as having a smaller value, i.e., P(X > Y) = P(Y > X). We chose this test because it does not assume equal variance between distributions, unlike the Mann–Whitney U test. The p-values vary with the number of samples, but the relationships across biomes and seasons remain robust and consistent with the distributions and their median values (see Suplementary Figs. 6–8).

The distinction between weak and strong fronts was intended to capture a more continuous gradient, reflecting the observation that the median distribution of total phytoplankton and most individual phytoplankton groups tends to increase progressively with higher heterogeneity index values (Supplementary Fig. 9). Therefore, the thresholds chosen for weak and strong fronts should be viewed as indicative and serve primarily to simplify the presentation of this increasing sensitivity to HI. To further validate our results, we subdivided each biome into narrower latitudinal bands to mitigate the potential influence of large-scale gradients on our analysis (Supplementary Figs. 10–12). We should note that although quantitative, this method is not mechanistic and does not able to distinguish between the processes at play.

#### Eveness of the phytoplankton community structure

We used the Shannon index to measure the evenness of the phytoplankton community structure (Evenness =  $-\sum_{i=1}^{N} P_i log(P_i)/log(N)$  where  $P_i$  is the relative concentration of each group and N=7 is the number of groups). The evenness is close to 1 when all groups are equally represented, and tends to 0 when one or a few groups dominate the community.

#### Dissimilary between phytoplankton communities

We computed the Bray–Curtis dissimilarity to measure the dissimilarity between pairs of communities a and b. (BC $^{a,b} = 1 - 2\sum_{i=1}^{N} \min(P_i^a, P_i^b) / \sum_{i=1}^{N} \left(P_i^a + P_i^b\right)$ . The Bray–Curtis dissimilarity is bounded between 0 and 1, where 0 means that the two communities have the same relative composition and 1 means that the two communities have completely different compositions. We computed the dissimilarity at the regional scale, between the median community composition of each pair of the three biomes. Then, within each biome, we computed the dissimilarity between strong fronts, weak fronts, and non-front conditions, by pair of each.

#### Data availability

The SST and Chl-a data used in this study were obtained from the Marine Data Store (MDS) of the E.U. Copernicus Marine Service Information (CMEMS). SST data are the ESA SST CCI and C3S reprocessed sea surface temperature analyses version 2.0 available at https://doi.org/10.48670/moi-00169<sup>112</sup>. Chl-a data are the Global Ocean Color (Copernicus-GlobColour), Bio-Geo-Chemical, L3 (daily) from Satellite Observations (1997-ongoing) produced by ACRI-ST, available at https://doi.org/10.48670/moi-00280<sup>113</sup>. We produced the HR data for phytoplankton groups. They are available at https://doi.org/10.5281/zenodo.14197394. The bathymetry data is the ETOPO1 60 Arc-Second Global Relief Model available at the NOAA National Centers for Environmental Information via https://doi.org/10.7289/V5C8276M<sup>114</sup>.

#### Code availability

Figures were created using Matplotlib version 3.8.1 available under a Matplotlib license at https://matplotlib.org<sup>115</sup>. Maps were created using Cartopy (0.22.0) available at https://doi.org/10.5281/zenodo.1182735under a BSD-3 license<sup>116</sup>; vector data for coastlines from Natural Earth https://www.naturalearthdata.com/; perceptually uniform colormaps from the package cmocean (2.0) at https://matplotlib.org/cmocean/<sup>117</sup>; and the package tolcolors (1.2.1) for color-blind safe color schemes, created by Paul Tol under a BSD-3 license and available at https://pypi.org/project/tol-colors/. The data analysis was performed with Xarray 2023.11 available at https://xarray.dev/<sup>118</sup>. The software to recreate figures is available on Zenodo at https://doi.org/10.5281/zenodo.15648847<sup>119</sup>.

Received: 20 December 2024; Accepted: 7 July 2025; Published online: 26 July 2025

#### References

- Karlusich, J. J. P., Ibarbalz, F. M. & Bowler, C. Exploration of marine phytoplankton: from their historical appreciation to the omics era. *J. Plankton Res.* 42, 595–612 (2020).
- Falkowski, P. The power of phytoplankton. *Nature* 483, S17–S20 (2012).
- Fenchel, T. The microbial loop 25 years later. J. Exp. Mar. Biol. Ecol. 366, 99–103 (2008).
- Fuhrman, J. A. Microbial community structure and its functional implications. *Nature* 459, 193–199 (2009).
- Guidi, L. et al. Effects of phytoplankton community on production, size, and export of large aggregates: a world-ocean analysis. *Limnol. Oceanogr.* 54, 1951–1963 (2009).
- Serra-Pompei, C. et al. Linking plankton size spectra and community composition to carbon export and its efficiency. Glob. Biogeochem. Cycles 36, e2021GB007275 (2022).
- Stukel, M. R. et al. Relationships between plankton size spectra, net primary production, and the biological carbon pump. *Glob. Biogeochem. Cycles* 38, e2023GB007994 (2024).
- Norberg, J. Phenotypic diversity and ecosystem functioning in changing environments: a theoretical framework. *Proc. Natl. Acad.* Sci. USA 98, 11376–11381 (2001).
- Bestion, E. et al. Phytoplankton biodiversity is more important for ecosystem functioning in highly variable thermal environments. *Proc. Natl. Acad. Sci.* 118, e2019591118 (2021).
- Abreu, A. et al. Priorities for ocean microbiome research. Nat. Microbiol. 7, 937–947 (2022).
- Schmidt, K. et al. Increasing picocyanobacteria success in shelf waters contributes to long-term food web degradation. Glob. Change Biol. 26, 5574–5587 (2020).
- Buttigieg, P. L. et al. Marine microbes in 4D—using time series observation to assess the dynamics of the ocean microbiome and its links to ocean health. *Curr. Opin. Microbiol.* 43, 169–185 (2018).
- Zhang, Z. et al. Global biogeography of microbes driving ocean ecological status under climate change. *Nat. Commun.* 15, 4657 (2024).
- Tréguer, P. et al. Influence of diatom diversity on the ocean biological carbon pump. Nat. Geosci. 11, 27–37 (2018).
- Busseni, G. et al. Large scale patterns of marine diatom richness: drivers and trends in a changing ocean. *Glob. Ecol. Biogeogr.* 29, 1915–1928 (2020).
- Wyatt, T. Margalef's mandala and phytoplankton bloom strategies. Deep-Sea Res. Part II Topical Stud. Oceanogr. 101, 32–49 (2014).
- Lewandowska, A. M., Striebel, M., Feudel, U., Hillebrand, H. & Sommer, U. The importance of phytoplankton trait variability in spring bloom formation. *ICES J. Mar. Sci.* 72, 1908–1915 (2015).

- Malviya, S. et al. Insights into global diatom distribution and diversity in the world's ocean. *Proc. Natl. Acad. Sci.* 113 https://doi.org/10. 1073/pnas.1509523113 (2016).
- Flombaum, P. et al. Present and future global distributions of the marine Cyanobacteria Prochlorococcus and Synechococcus. *Proc. Natl. Acad. Sci. USA* 110, 9824–9829 (2013).
- Ribeiro, K. F., Duarte, L. & Crossetti, L. O. Everything is not everywhere: a tale on the biogeography of cyanobacteria. *Hydrobiologia* 820, 23–48 (2018).
- Rousset, G. et al. Remote sensing of *Trichodesmium* spp. mats in the western tropical South Pacific. *Biogeosciences* 15, 5203–5219 (2018).
- Cheung, S. et al. Physical forcing controls the basin-scale occurrence of nitrogen-fixing organisms in the North Pacific Ocean. Glob. Biogeochem. Cycles 34, 1–12 (2020).
- Belkin, I. M., Cornillon, P. C. & Sherman, K. Fronts in large marine ecosystems. *Prog. Oceanogr.* 81, 223–236 (2009).
- Lévy, M., Franks, P. J. S. & Smith, K. S. The role of submesoscale currents in structuring marine ecosystems. *Nat. Commun.* 9 http:// www.nature.com/articles/s41467-018-07059-3 (2018).
- Thomas, L. N., Tandon, A. & Mahadevan, A. Submesoscale processes and dynamics. In Hecht, M. W. & Hasumi, H. (eds.) Geophysical Monograph Series, vol. 177, 17–38 (American Geophysical Union, 2008). https://doi.org/10.1029/177GM04
- McWilliams, J. C. Submesoscale currents in the ocean. Proc. R. Soc. A Math. Phys. Eng. Sci. 472, 20160117 (2016).
- Mahadevan, A. The impact of submesoscale physics on primary productivity of plankton. Annu. Rev. Mar. Sci. 8, 161–184 (2016).
- Mahadevan, A. et al. Coherent pathways for vertical transport from the surface ocean to interior. *Bull. Am. Meteorol. Soc.* 101, E1996–E2004 (2020).
- Franks, P. J. Sink or swim: accumulation of biomass at fronts. *Mar. Ecol. Prog. Ser. Oldendorf* 82, 1–12 (1992).
- Allen, J. T. et al. Diatom carbon export enhanced by silicate upwelling in the northeast Atlantic. *Nature* 437, 728–732 (2005).
- 31. Ribalet, F. et al. Unveiling a phytoplankton hotspot at a narrow boundary between coastal and offshore waters. *Proc. Natl. Acad. Sci. USA* **107**, 16571–16576 (2010).
- d'Ovidio, F., De Monte, S., Alvain, S., Dandonneau, Y. & Levy, M. Fluid dynamical niches of phytoplankton types. *Proc. Natl. Acad. Sci. USA* 107, 18366–18370 (2010).
- 33. Romero, O. E., Fischer, G., Karstensen, J. & Cermeño, P. Eddies as trigger for diatom productivity in the open-ocean Northeast Atlantic. *Prog. Oceanogr.* **147**, 38–48 (2016).
- 34. Oliver, H. et al. Diatom hotspots driven by western boundary current instability. *Geophys. Res. Lett.* **48**, e2020GL091943 (2021).
- Hernández-Carrasco, I. et al. Flow structures with high Lagrangian coherence rate promote diatom blooms in oligotrophic waters. Geophys. Res. Lett. 50, e2023GL103688 (2023).
- Mangolte, I., Lévy, M., Haëck, C. & Ohman, M. D. Sub-frontal niches of plankton communities driven by transport and trophic interactions at ocean fronts. *Biogeosciences* 20, 3273–3299 (2023).
- Lévy, M. et al. The impact of fine-scale currents on biogeochemical cycles in a changing ocean. *Annu. Rev. Mar. Sci.* 16, annurev– marine–020723–020531 (2024).
- Kahru, M., Di Lorenzo, E., Manzano-Sarabia, M. & Mitchell, B. G. Spatial and temporal statistics of sea surface temperature and chlorophyll fronts in the California Current. *J. Plankton Res.* 34, 749–760 (2012).
- Gaube, P., McGillicuddy, D. J., Chelton, D. B., Behrenfeld, M. J. & Strutton, P. G. Regional variations in the influence of mesoscale eddies on near-surface chlorophyll. *J. Geophys. Res. Oceans* 119, 8195–8220 (2014).
- Liu, X. & Levine, N. M. Enhancement of phytoplankton chlorophyll by submesoscale frontal dynamics in the North Pacific Subtropical Gyre. Geophys. Res. Lett. 43, 1651–1659 (2016).

- Guo, M., Xiu, P., Chai, F. & Xue, H. Mesoscale and submesoscale contributions to high sea surface Chlorophyll in subtropical gyres. *Geophys. Res. Lett.* 46, 13217–13226 (2019).
- Haëck, C., Lévy, M., Mangolte, I. & Bopp, L. Satellite data reveal earlier and stronger phytoplankton blooms over fronts in the Gulf Stream region. *Biogeosciences* 20, 1741–1758 (2023).
- McKee, D. C. et al. Biophysical dynamics at ocean fronts revealed by bio-argo floats. *J. Geophys. Res. Oceans* 128, e2022JC019226 (2023).
- El Hourany, R. et al. Estimation of secondary phytoplankton pigments from satellite observations using Self-Organizing Maps (SOMs). J. Geophys. Res. Oceans 124, 1357–1378 (2019).
- Vidussi, F., Claustre, H., Manca, B. B., Luchetta, A. & Marty, J.-C. Phytoplankton pigment distribution in relation to upper thermocline circulation in the eastern Mediterranean Sea during winter. *J. Geophys. Res. Oceans* 106, 19939–19956 (2001).
- Dugenne, M., Henderikx Freitas, F., Wilson, S. T., Karl, D. M. & White, A. E. Life and death of Crocosphaera sp. in the Pacific Ocean: fine scale predator–prey dynamics. *Limnol. Oceanogr.* 65, 2603–2617 (2020).
- Tzortzis, R. et al. Impact of moderately energetic fine-scale dynamics on the phytoplankton community structure in the western Mediterranean Sea. *Biogeosciences* 18, 6455–6477 (2021).
- Benavides, M. et al. Fine-scale sampling unveils diazotroph patchiness in the South Pacific Ocean. ISME Commun. 1, 3 (2021).
- Tzortzis, R. et al. The contrasted phytoplankton dynamics across a frontal system in the southwestern Mediterranean Sea. *Biogeosciences* 20, 3491–3508 (2023).
- Alvain, S., Moulin, C., Dandonneau, Y. & Loisel, H. Seasonal distribution and succession of dominant phytoplankton groups in the global ocean: a satellite view. *Glob. Biogeochem. Cycles* 22, 1–15 (2008).
- Xi, H. et al. Global chlorophyll a concentrations of phytoplankton functional types with detailed uncertainty assessment using multisensor ocean color and sea surface temperature satellite products. J. Geophys. Res. Oceans 126, 1–27 (2021).
- Aiken, J. et al. Phytoplankton pigments and functional types in the Atlantic Ocean: a decadal assessment, 1995–2005. Deep Sea Res. Part II Topical Stud. Oceanogr. 56, 899–917 (2009).
- Acevedo-Trejos, E., Marañón, E. & Merico, A. Phytoplankton size diversity and ecosystem function relationships across oceanic regions. *Proceedings of the Royal Society B: Biological Sciences* 285, 29794050 (2018).
- Boyce, D. G., Petrie, B., Frank, K. T., Worm, B. & Leggett, W. C. Environmental structuring of marine plankton phenology. *Nat. Ecol. Evol.* 1, 1484–1494 (2017).
- Sommeria-Klein, G. et al. Global drivers of eukaryotic plankton biogeography in the sunlit ocean. Science 374, 594–599 (2021).
- Richter, D. J. et al. Genomic evidence for global ocean plankton biogeography shaped by large-scale current systems. *eLife* 11, 1–38 (2022).
- 57. Dutkiewicz, S. et al. Dimensions of marine phytoplankton diversity. *Biogeosciences* **17**, 609–634 (2020).
- Lévy, M. et al. Production regimes in the northeast Atlantic: a study based on Sea-viewing Wide Field-of-view Sensor (SeaWiFS) chlorophyll and ocean general circulation model mixed layer depth. J. Geophys. Res. Oceans 110 https://doi.org/10.1029/2004JC002771 (2005).
- Raes, E. J. et al. Oceanographic boundaries constrain microbial diversity gradients in the South Pacific Ocean. *Proc. Natl. Acad. Sci.* 115 https://doi.org/10.1073/pnas.1719335115 (2018).
- Juranek, L. W. et al. The importance of the phytoplankton "middle class" to ocean net community production. *Glob. Biogeochem.* Cycles 34, e2020GB006702 (2020).

- Sturm, D., Morton, P., Langer, G., Balch, W. M. & Wheeler, G. Latitudinal gradients and ocean fronts strongly influence protist communities in the southern Pacific Ocean. FEMS Microbiol. Ecol. 100. fiae137 (2024).
- 62. Liang, X., Spall, M. & Wunsch, C. Global ocean vertical velocity from a dynamically consistent ocean state estimate. *J. Geophys. Res. Oceans* **122**, 8208–8224 (2017).
- 63. Williams, R. G. & Follows, M. Ocean Dynamics and the Carbon Cycle: Principles and Mechanisms (Cambridge University Press, 2011).
- Spingys, C. P. et al. Observations of nutrient supply by mesoscale eddy stirring and small-scale turbulence in the oligotrophic North Atlantic. *Glob. Biogeochem. Cycles* 35, e2021GB007200 (2021).
- de Boyer Montégut, C., Madec, G., Fischer, A. S., Lazar, A. & Iudicone,
  D. Mixed layer depth over the global ocean: an examination of profile data and a profile-based climatology. *J. Geophys. Res. Oceans* 109 https://doi.org/10.1029/2004JC002378 (2004).
- Alexander, H. et al. Functional group-specific traits drive phytoplankton dynamics in the oligotrophic ocean. *Proc. Natl. Acad.* Sci. 112 https://doi.org/10.1073/pnas.1518165112 (2015).
- 67. Rivière, P. & Pondaven, P. Phytoplankton size classes competitions at sub-mesoscale in a frontal oceanic region. *J. Mar. Syst.* **60**, 345–364 (2006).
- Lévy, M., Jahn, O., Dutkiewicz, S., Follows, M. J. & d'Ovidio, F. The dynamical landscape of marine phytoplankton diversity. *J. R. Soc. Interface* 12, 20150481 (2015).
- Mangolte, I., Lévy, M., Dutkiewicz, S., Clayton, S. & Jahn, O. Plankton community response to fronts: winners and losers. *J. Plankton Res.* 44, 241–258 (2022).
- Pelegrí, J. L., Vallès-Casanova, I. & Orúe-Echevarría, D. The Gulf Nutrient Stream. Geophysical Monograph Series (Wiley & Sons American Geophysical Union, 2019).
- Incze, L. S. & Yentsch, C. M. Stable density fronts and dinoflagellate patches in a tidal estuary. *Estuar., Coast. Shelf Sci.* 13, 547–556 (1981).
- Pitcher, G. C., Boyd, A. J., Horstman, D. A. & Mitchell-Innes, B. A. Subsurface dinoflagellate populations, frontal blooms and the formation of red tide in the southern Benguela upwelling system. *Mar. Ecol. Prog. Ser.* 172, 253–264 (1998).
- Gravalosa, J. M., Flores, J. A., Sierro, F. J. & Gersonde, R. Sea surface distribution of coccolithophores in the eastern Pacific sector of the Southern Ocean (Bellingshausen and Amundsen Seas) during the late austral summer of 2001. *Mar. Micropaleontol.* 69, 16–25 (2008)
- Saavedra-Pellitero, M., Baumann, K.-H., Flores, J.-A. & Gersonde, R. Biogeographic distribution of living coccolithophores in the Pacific sector of the Southern Ocean. *Mar. Micropaleontol.* 109, 1–20 (2014).
- Taylor, A. G. et al. Sharp gradients in phytoplankton community structure across a frontal zone in the California Current Ecosystem. *J. Plankton Res.* 34, 778–789 (2012).
- Marrec, P. et al. Coupling physics and biogeochemistry thanks to high-resolution observations of the phytoplankton community structure in the northwestern Mediterranean Sea. *Biogeosciences* 15, 1579–1606 (2018).
- Palter, J. B. et al. High N2 fixation in and near the Gulf Stream consistent with a circulation control on diazotrophy. *Geophys. Res. Lett.* 47, e2020GL08910 (2020).
- Hoerstmann, C. et al. Nitrogen fixation in the North Atlantic supported by Gulf Stream eddy-borne diazotrophs. *Nat. Geosci.* 17, 1141–1147 (2024).
- Cavicchioli, R. et al. Scientists' warning to humanity: microorganisms and climate change. *Nat. Rev. Microbiol.* 17, 569–586 (2019).
- Bopp, L., Aumont, O., Cadule, P., Alvain, S. & Gehlen, M. Response of diatoms distribution to global warming and potential implications:

- a global model study. *Geophys. Res. Lett.* **32** https://doi.org/10. 1029/2005GL023653 (2005).
- 81. Morán, X. A. G., López-Urrutia, n, Calvo-Díaz, A. & Li, W. K. W. Increasing importance of small phytoplankton in a warmer ocean. *Glob. Change Biol.* **16**, 1137–1144 (2010).
- Barton, A. D., Irwin, A. J., Finkel, Z. V. & Stock, C. A. Anthropogenic climate change drives shift and shuffle in North Atlantic phytoplankton communities. *Proc. Natl. Acad. Sci. USA* 113, 2964–2969 (2016).
- Sommer, U., Peter, K. H., Genitsaris, S. & Moustaka-Gouni, M. Do marine phytoplankton follow Bergmann's rule sensu lato? *Biol. Rev.* 92, 1011–1026 (2017).
- Wei, Y. et al. Temperature and nutrients drive distinct successions between diatoms and dinoflagellates over the past 40 years: implications for climate warming and eutrophication. Sci. Total Environ. 931, 172997 (2024).
- Kwiatkowski, L., Aumont, O. & Bopp, L. Consistent trophic amplification of marine biomass declines under climate change. *Glob. Change Biol.* 25, 218–229 (2019).
- Du Pontavice, H., Gascuel, D., Reygondeau, G., Stock, C. & Cheung, W. W. L. Climate-induced decrease in biomass flow in marine food webs may severely affect predators and ecosystem production. *Glob. Change Biol.* 27, 2608–2622 (2021).
- Martinetto, P. et al. Linking the scientific knowledge on marine frontal systems with ecosystem services. *Ambio* 49, 541–556 (2020).
- Miller, P. I. & Christodoulou, S. Frequent locations of oceanic fronts as an indicator of pelagic diversity: application to marine protected areas and renewables. *Mar. Policy* 45, 318–329 (2014).
- Scales, K. L. et al. On the front line: frontal zones as priority at-sea conservation areas for mobile marine vertebrates. *J. Appl. Ecol.* 51, 1575–1583 (2014).
- Della Penna, A. et al. Lagrangian analysis of multi-satellite data in support of open ocean Marine Protected Area design. *Deep-Sea Res. Part II Topical Stud. Oceanogr.* 140, 212–221 (2017).
- 91. Prants, S. V. Fisheries at Lagrangian fronts. *Fish. Res.* **279**, 107125 (2024).
- Matear, R. J., Chamberlain, M. A., Sun, C. & Feng, M. Climate change projection of the Tasman Sea from an Eddy-resolving Ocean Model. J. Geophys. Res. Oceans 118, 2961–2976 (2013).
- Martínez-Moreno, J. et al. Global changes in oceanic mesoscale currents over the satellite altimetry record. *Nat. Clim. Change* 11, 397–403 (2021).
- Richards, K. J. et al. The impact of climate change on ocean submesoscale activity. J. Geophys. Res. Oceans 126, 1–15 (2021).
- Yang, K., Meyer, A., Strutton, P. G. & Fischer, A. M. Global trends of fronts and chlorophyll in a warming ocean. *Commun. Earth Environ.* 4, 1–11 (2023).
- Xing, Q., Yu, H. & Wang, H. Global mapping and evolution of persistent fronts in Large Marine Ecosystems over the past 40 years. Nat. Commun. 15, 38744883 (2024).
- Setta, S. P., Lerch, S., Jenkins, B. D., Dyhrman, S. T. & Rynearson, T. A. Oligotrophic waters of the Northwest Atlantic support taxonomically diverse diatom communities that are distinct from coastal waters. *J. Phycol.* 59, 1202–1216 (2023).
- Leblanc, K. et al. Nanoplanktonic diatoms are globally overlooked but play a role in spring blooms and carbon export. *Nat. Commun.* 9, 953 (2018).
- Arsenieff, L. et al. Diversity and dynamics of relevant nanoplanktonic diatoms in the Western English Channel. ISME J. 14, 1966–1981 (2020).
- Lehahn, Y., d'Ovidio, F., Lévy, M. & Heifetz, E. Stirring of the Northeast Atlantic spring bloom: a Lagrangian analysis based on multisatellite data. J. Geophys. Res. Oceans 112 https://doi.org/10. 1029/2006JC003927 (2007).

- Merchant, C. J. et al. Satellite-based time-series of sea-surface temperature since 1981 for climate applications. Sci. Data 6, 223 (2019).
- Good, S. et al. The current configuration of the OSTIA system for operational production of foundation sea surface temperature and ice concentration analyses. *Remote Sens.* 12, 720 (2020).
- 103. Garnesson, P., Mangin, A., Fanton d'Andon, O., Demaria, J. & Bretagnon, M. The CMEMS GlobColour chlorophyll a product based on satellite observation: multi-sensor merging and flagging strategies. *Ocean Sci.* 15, 819–830 (2019).
- Stoer, A. C. & Fennel, K. Carbon-centric dynamics of Earth's marine phytoplankton. *Proc. Natl. Acad. Sci. USA* 121, e2405354121 (2024).
- El Hourany, R. et al. Linking satellites to genes with machine learning to estimate phytoplankton community structure from space. *Ocean* Sci. 20, 217–239 (2024).
- Uitz, J., Claustre, H., Morel, A. & Hooker, S. B. Vertical distribution of phytoplankton communities in open ocean: an assessment based on surface chlorophyll. *J. Geophys. Res.* 111 https://doi.org/10. 1029/2005JC003207 (2006).
- Soppa, M. A. et al. Global retrieval of diatom abundance based on phytoplankton pigments and satellite data. *Remote Sens.* 6, 10089–10106 (2014).
- Brewin, R. J. W. et al. Influence of light in the mixed-layer on the parameters of a three-component model of phytoplankton size class. *Remote Sens. Environ.* 168, 437–450 (2015).
- Chase, A. P. et al. Evaluation of diagnostic pigments to estimate phytoplankton size classes. *Limnol. Oceanogr. Methods* 18, 570–584 (2020).
- Gangrade, S. & Mangolte, I. Patchiness of plankton communities at fronts explained by Lagrangian history of upwelled water parcels. *Limnol. Oceanogr.* 69, 2123–2137 (2024).
- Brunner, E. & Munzel, U. The nonparametric Behrens-Fisher problem: asymptotic theory and a small-sample approximation. *Biometrical J.* 42. 17–25 (2000).
- E.U., Copernicus Marine Service Information (CMEMS). Marine Data Store (MDS). ESA SST CCI and C3S reprocessed sea surface temperature analyses https://data.marine.copernicus.eu/product/ SST\_GLO\_SST\_L4\_REP\_OBSERVATIONS\_010\_024 (2019).
- E.U., Copernicus Marine Service Information (CMEMS). Marine Data Store (MDS). Global Ocean Colour (Copernicus-GlobColour), Bio-Geo-Chemical, L3 (daily) from Satellite Observations (1997ongoing) https://resources.marine.copernicus.eu/product-detail/ OCEANCOLOUR\_GLO\_BGC\_L3\_MY\_009\_103/INFORMATION (2022).
- 114. NOAA National Geophysical Data Center. ETOPO1 1 Arc-Minute Global Relief Model https://data.nodc.noaa.gov/cgi-bin/iso?id= gov.noaa.ngdc.mgg.dem:316 (2009).
- 115. Hunter, J. D. Matplotlib: a 2D graphics environment. *Comput. Sci. Eng.* **9**, 90–95 (2007).
- Met Office. Cartopy: a cartographic Python library with a Matplotlib interface [Software] https://scitools.org.uk/cartopy (2015).
- Thyng, K., Greene, C., Hetland, R., Zimmerle, H. & DiMarco, S. True colors of oceanography: guidelines for effective and accurate colormap selection. *Oceanography* 29, 9–13 (2016).
- Hoyer, S. & Hamman, J. Xarray: N-D labeled arrays and datasets in Python. J. Open Res. Softw. 5 https://doi.org/10.5334/jors.148 (2017).
- Haëck, C. Shift in phytoplankton community composition over fronts [Code and Data] https://doi.org/10.5281/zenodo.15648846 (2025).

#### Acknowledgements

This study was supported by CNES (Biofront project), ESA (4D-Medsea project) and the Chanel chair of ENS. The project benefited from the

resources of the mesocentre ESPRI of IPSL. We thank Laure Resplandy for useful feedbacks on a preliminary version of the manuscript, and three anonymous reviewers for their constructive comments.

#### **Author contributions**

M.L. designed research; C.H. performed research; M.L., I.M., C.H.H. and A.C. analysed data; R.E. produced data; M.L. and I.M. wrote the paper.

#### **Competing interests**

The authors declare no competing interests.

#### **Additional information**

**Supplementary information** The online version contains supplementary material available at https://doi.org/10.1038/s43247-025-02553-1.

**Correspondence** and requests for materials should be addressed to Marina Lévy.

**Peer review information** Communications Earth & Environment thanks Diana N. Fontaine and the other, anonymous, reviewer(s) for their contribution to the peer review of this work. Primary Handling Editors: Alice Drinkwater and Mengjie Wang. [A peer review file is available].

Reprints and permissions information is available at http://www.nature.com/reprints

**Publisher's note** Springer Nature remains neutral with regard to jurisdictional claims in published maps and institutional affiliations.

Open Access This article is licensed under a Creative Commons Attribution-NonCommercial-NoDerivatives 4.0 International License, which permits any non-commercial use, sharing, distribution and reproduction in any medium or format, as long as you give appropriate credit to the original author(s) and the source, provide a link to the Creative Commons licence, and indicate if you modified the licensed material. You do not have permission under this licence to share adapted material derived from this article or parts of it. The images or other third party material in this article are included in the article's Creative Commons licence, unless indicated otherwise in a credit line to the material. If material is not included in the article's Creative Commons licence and your intended use is not permitted by statutory regulation or exceeds the permitted use, you will need to obtain permission directly from the copyright holder. To view a copy of this licence, visit http://creativecommons.org/licenses/by-nc-nd/4.0/.

© The Author(s) 2025